Disentangling the Galaxy's Gordian knot: evidence from APOGEE-Gaia for a knotted and slower bar in the Milky Way

Horta et al. (2023)　arXiv: 2402.07986

2024.02.19 (Mon)　服部公平

概要　Gaia/APOGEE dataを用いて、銀河系の半径R<5 kpc のinner Galaxyの運動・化学組成情報を調べた。
軌道角運動量を用いた分類で、inner Galaxy の星はbar, disk, **knot**の３成分に分類できる(ハローは除外)。
knot は(i) 空間分布は回転楕円体; (ii) R<1.5 kpcで高密度; (iii) nearly radial orbit卓越; (iv) super-Solar [Fe/H];
で特徴づけられる。化学組成は3者は似ているので、起源は同じだろう。knotは「secular evolution(永年進化)
で形成されたが、(pseudo bulgeではなく)classical bulgeに類似した成分」と考えられる。
また、bar 成分の運動は従来より遅いbarである可能性を示唆(pattern speed = 24+/-3 km/s/kpc)。

ゴール　**R<5 kpc の inner Galaxyの化学動力学構造を観測的に調べる。**

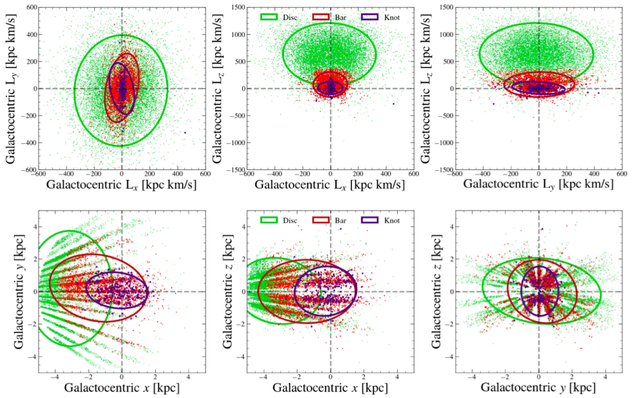
オリジナリティ　**Classical bulgeの新たな範疇になるかもしれないknot成分を提唱。**

データ　**Gaia/APOGEEのクロスマッチカタログ(N=65万天体)から、高精度サンプルN=18,933を選択。**

結果1

- **(Lx, Ly, Lz)-空間でのGMMでサンプルを3成分fit。**
- **Knot成分はLz~0 で、radial orbitが卓越。**

… 空間的な広がりは1-1.5 kpc程度。



上段：角運動量分布。下段：空間分布。
Disk, Bar, Knotの色分けはGMMの確率分布に基づく。

結果2

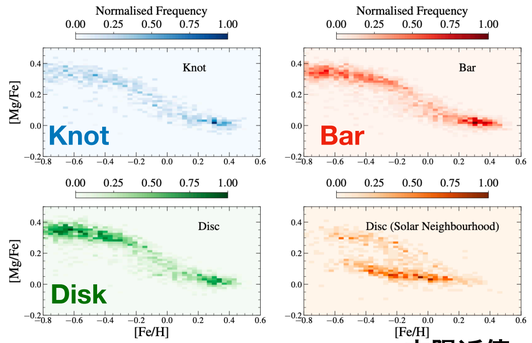
- **inner Galaxyの3成分とも、単一のtrackを示す。**
- **high-alpha, low-alphaの個数分布こそ僅かに異なるが、年齢も7-12 Gyrと酷似(本資料2ページ)。**

… 3成分は同じような時間スケールで形成された。
… secular evolutionを示唆。

- **太陽近傍の分布とは大きく異なる。**

… 先行研究(Bensby+2017)とは異なる年齢分布(4ページ).
… Bensby+2017のサンプルは近傍星のcontamination?

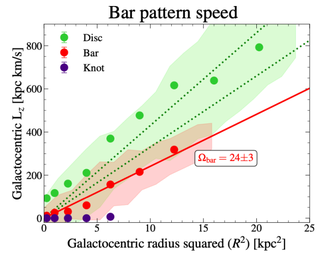
- **論文に図はないが、Mg以外の元素でも同様のトレンド。**



結果3

- **bar 成分のLz-Rの分布からパターン速度を推定。**

… Omega_bar = 24+/- 3 km/s/kpc (かなり遅い)
… 先行研究はbarにトラップされていない星のcontaminationがあるかもしれないと主張。
… Mock data analysisで有用性を確認(本資料3ページ)。



議論１

- **バルジ領域の先行研究(-1.5<[Fe/H]<0.4; 8-10Gyr < age)と整合的。**
- **バルジ領域のハロー星(Heraclesなど)は今回は[Fe/H]-cutのため触れていない。**

議論２

- **knotはorbit的にはclassical bulgeだが、化学組成は典型的なclassical bulgeとは相反する。**
- **一般的なclassical bulgeはmerger-drivenとされる。MWにおいては、MW中心付近のHeracles構造(metal-poorな矮小銀河残骸)がちょうどclassical bulgeの描像に当てはまる。**
- **knotは、classical bulgeの範疇でありつつ、metal-richである。**
- **knotは、classical bulgeの新たなタイプとみなせるかもしれない。**

	Radial orbit	Age	Chemistry	起源
classical bulge	O	old	metal-poor	merger
pseudo bulge	X	diskと同じ	diskと同じ	secular
Knot	O	old	metal-rich	secular

コメント１

Bensby et al. (2017; pre-Gaiaの時代)の"bulge sample"について、Gaia の運動データから
foreground disk stars / real bulge stars の判別を行えば、bulge stars の年齢分布について
今回の論文が正しいかどうかクリアになるかもしれない。

コメント２

snapshotからpattern speedを出す手法をDehnenが最近出版しているが、その手法では
「barにtrapされている」などの選択をせずに星を全部使ってpattern speedを計算している。
本論文の手法との本質的な違いが気になる。
今回の手法はmock dataで有効性を確認している。そのmock dataにDehnenの手法を使ったら何が起きる？

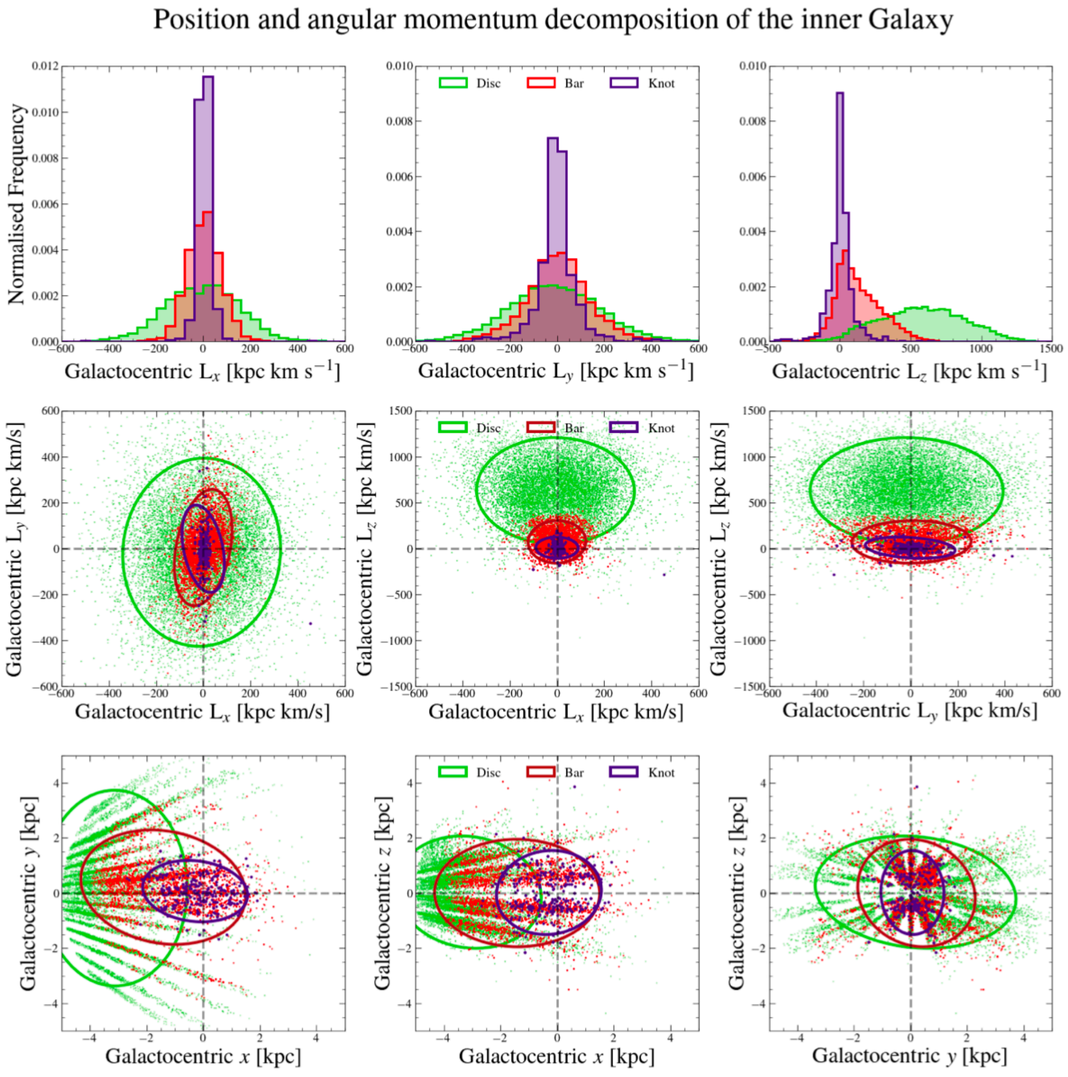


Figure 2. *Top row*: Normalised angular momentum distribution of the parent sample weighted by the probability of stars being associated with the knot (blue), bar (red), and disc (green). *Middle row*: Angular momentum distribution of the three samples identified using our angular momentum decomposition Gaussian mixture likelihood method with their corresponding 2σ confidence ellipse. Here, the confidence ellipse should not be interpreted as the Gaussian fits to the data, but are instead to guide the eye as to the extent of each component. The distribution of these components is much tighter in angular momentum space than in position space, making it easier to dissect stellar populations in the inner Galaxy. For these and the bottom row, only stars with high probability of them being associated with their respective components are shown (i.e., $p > 0.8$). The knot component shows a much tighter distribution in angular momentum, centred around $\mathbf{L} \sim 0$ kpc km s^{-1}. *Bottom row*: Galactocentric Cartesian coordinate projections of the three components (disc, bar, and knot) identified with the angular momentum decomposition with their corresponding 2σ confidence ellipses. The *APOGEE* pencil-beam footprint is clearly apparent, making any identification in $[x, y, z]$ space challenging. In the middle and bottom rows the cross-hair corresponds to the position of the Galactic centre.

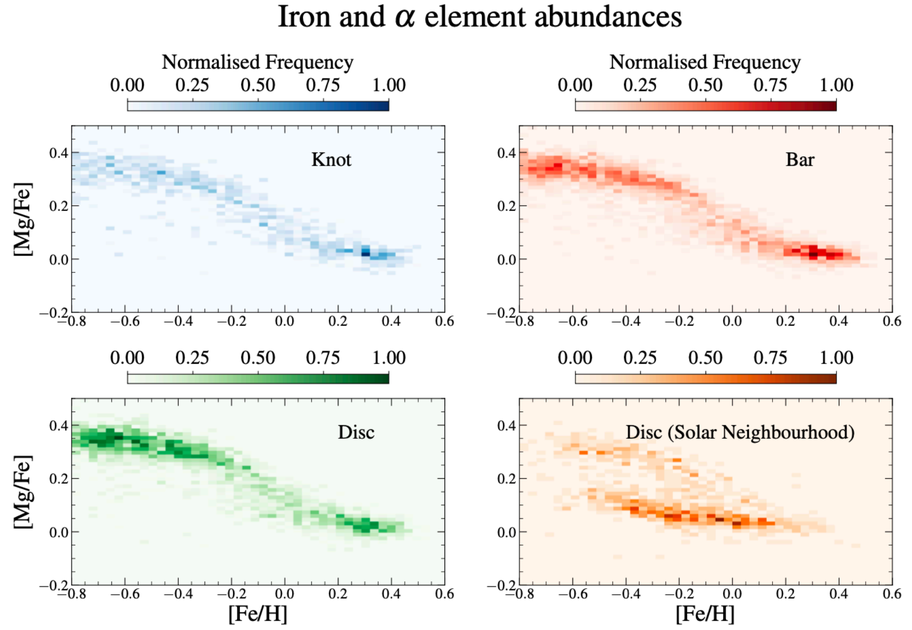


Figure 3. Median [Mg/Fe]-[Fe/H] density distributions for the knot (top left), bar (top right), and inner disc (bottom left) samples from 20 posterior chains of probability values computed using the angular momentum Gaussian mixture model decomposition procedure. Only stars within $R < 3$ kpc and $1.5 > \log g > 0.5$ are shown in the knot, bar, and inner disc panels, to account for systematic trends with surface gravity in our element abundance measurements. For reference, we also show disc populations in the solar neighbourhood (bottom right), defined the same way as the knot/bar/inner disc sample but for stars with heliocentric distances smaller than $d_\odot < 2$ kpc (again, only showing stars with $1.5 > \log g > 0.5$). The knot, bar, and inner disc samples follow a single track in the α-Fe plane. All three populations show a trough in [Mg/Fe] at [Fe/H] $\sim$ solar, and are vastly different from disc populations in the solar neighbourhood; the solar neighbourhood sample also displays the known disc α-Fe bimodality (Hayden et al. 2015), which is not seen for inner Galaxy populations. The inner disc sample shows a higher fraction of stars in the high-[Mg/Fe] sequence than the bar and knot (see also Fig 4). The similar chemical abundances between the knot, bar, and inner disc suggests that these populations share a similar star formation history and likely formed over similar timescales. Thus, the chemical compositions of these three samples indicate that they are likely related. The different abundances between the inner and solar neighbourhood discs suggests different star formation histories. The higher [Fe/H] abundances of the inner disc suggests that it formed more rapidly and with a higher star formation rate/efficiency when compared to the disc in the solar neighbourhood, in contrast to recent studies (Bovy et al. 2019).

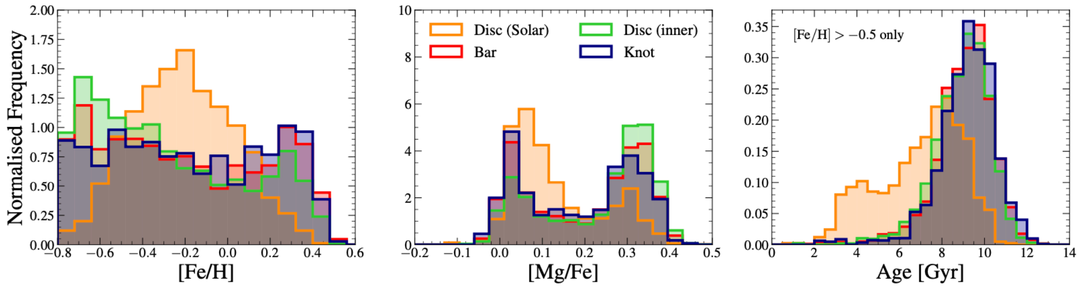


Figure 4. Normalised histogram distributions of [Fe/H] (*left*), [Mg/Fe] (*middle*), and age (*right*) for stars in the knot, bar, inner disc, and solar neighbourhood disc. Only stars with $0.5 < \log g < 1.5$ are used, to ensure no metallicity gradients and/or systematic effects in the abundances. Moreover, for the right panel, a cut of [Fe/H]> -0.5 is performed to ensure trustworthy ages, as below this metallicity there were no stars in the training sample used in *astroNN*. The inner disc sample is dominated by stars that are more [Fe/H]-poor and have higher [Mg/Fe] abundances when compared to the bar/knot. This is also the case when comparing the bar to the knot, although the differences are more subtle. In fact, there is a gradient in α-Fe, whereby the distribution for the knot is weighted to lower [Mg/Fe], the bar sits in between the knot and inner disc, and the inner disc is weighted towards more enhanced [Mg/Fe] abundances. We find that the age distribution of the knot, bar, and inner disc are all qualitatively the same, and are comprised by old stars (Age $\gtrsim 7$ Gyr). The abundances and ages of the solar neighbourhood disc are vastly different to the inner Galaxy populations, in contrast to recent findings using similar data (Bovy et al. 2019).

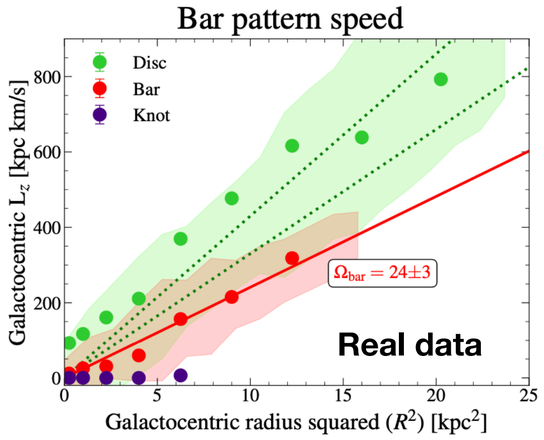


Figure 5. Azimuthal angular momentum as a function of Galactocentric radius squared. Markers show the values for the centroids of our model fits, whereas shaded regions show the 16^{th} and 84^{th} percentile range for the data with a probability of being associated to the bar (red) and inner disc (green) greater than $p > 0.8$. The red line is a linear regression fit to the fitted L_z values for the bar component in independent radius bins, where the uncertainty is computed using the scatter in the corresponding L_z values (i.e., σ_{L_z}). We note that we also fitted the full data of bar member stars weighted by $p_{\rm bar}$ (i.e., a weighted fit to the bar sample), and found the same $\Omega_{\rm bar}$ value. The dashed green lines are linear models with slopes that match the high and low estimates of the pattern speed from previous works ($\Omega_{\rm bar} = [33, 43]$ km s^{-1} kpc^{-1}). The fit to the bar sample yields a value for the pattern speed of $\Omega_{\rm bar} = 24 \pm 3$ km s^{-1} kpc^{-1}. This value is lower than recent estimates (Portail et al. 2017; Bovy et al. 2019; Sanders et al. 2019), which we find more closely agree with the inner disc data (green).

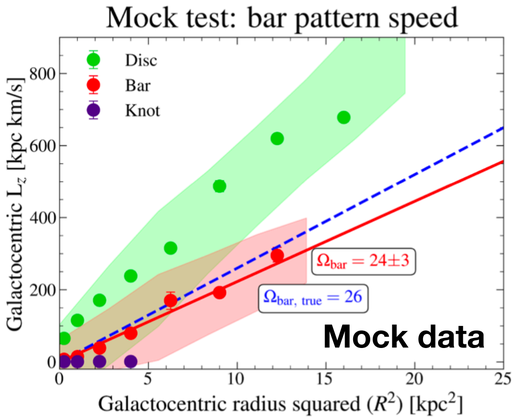


Figure A3. Measurements of the pattern speed of the bar in the mock *APOGEE* data set. The layout is the same as Figure 5. Given that we know the true values for the mock data set, we are able to compare the fit parameters with the true values.

Mock data analysis.
bar 成分だけを取り出すと、

正しいpattern speedが出ると主張。

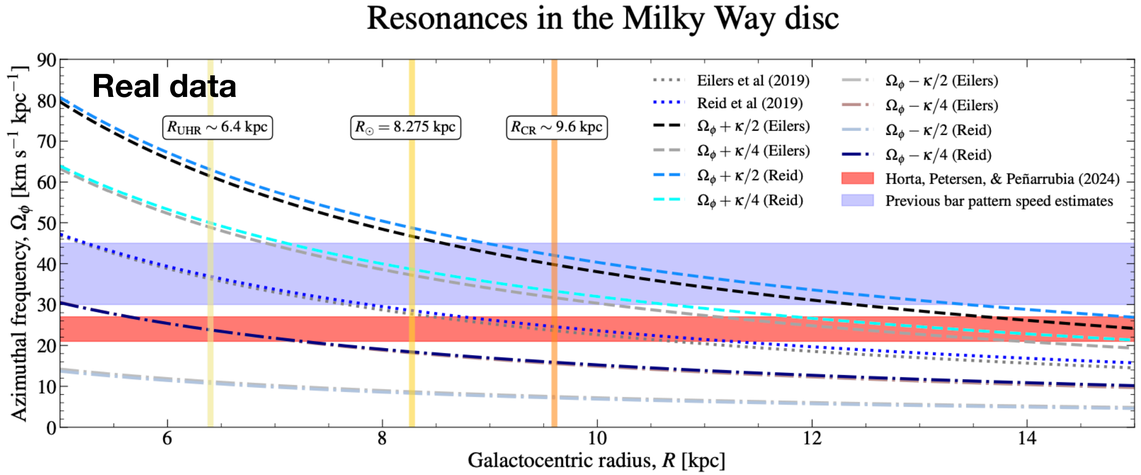
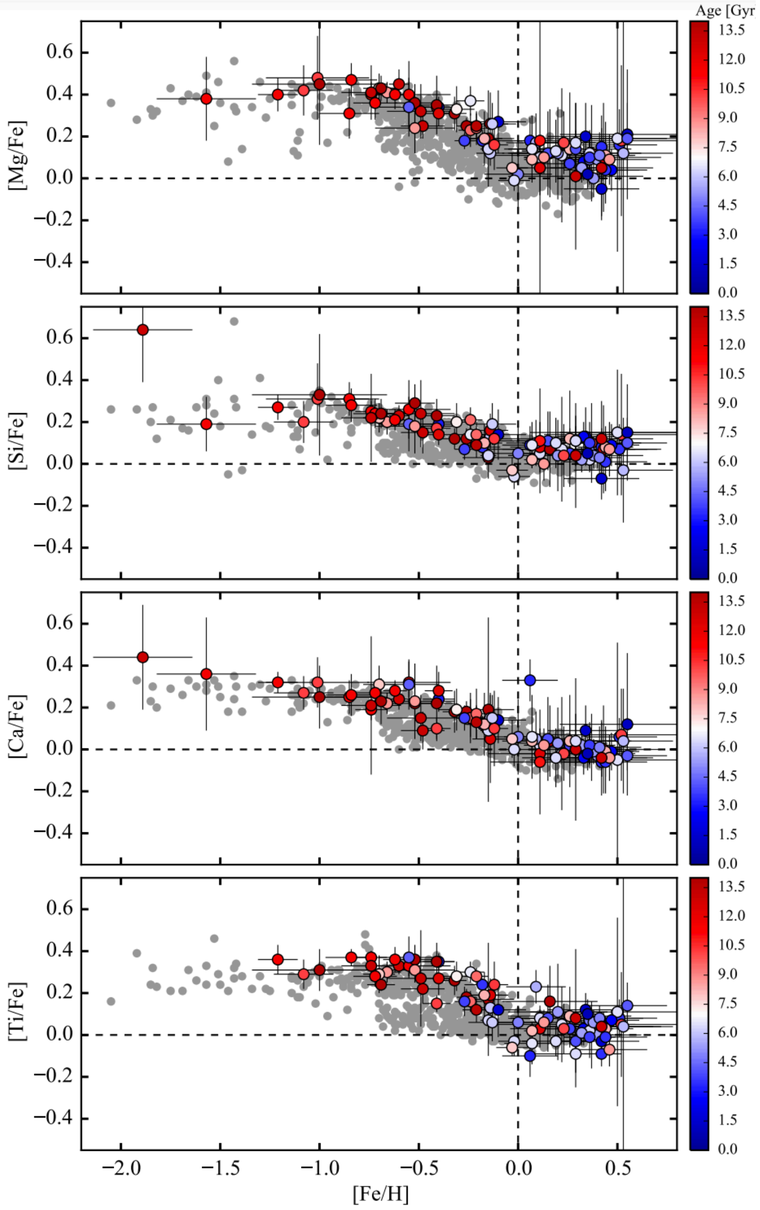


Figure 6. Azimuthal frequency as a function of (cylindrical) Galactocentric radius. Shown as dotted lines are the curves computed assuming the rotation curve of the Milky Way from Eilers et al. (2019) (gray) and Reid et al. (2019) (blue). As dashed (dashed-dotted) lines we also show the profiles of the positive (negative) resonance condition curves ($\Omega_{\rm bar} \pm \kappa/2$ or $\Omega_{\rm bar} \pm \kappa/4$). As a shaded red line we show the range of azimuthal frequencies we measure in this work for the Milky Way bar's pattern speed, $\Omega_{\rm bar} = 24 \pm 3$ km s^{-1} kpc^{-1}. For comparison, as a blue shaded region we show the range in values for $\Omega_{\rm bar}$ reported in previous studies. The radius at which the dotted line crosses the value of the bar's pattern speed marks the corotation radius, which we estimate to be $R_{\rm CR} \sim 9.4$ kpc using the Eilers et al. (2019) rotation curve, and $R_{\rm CR} \sim 9.8$ kpc using the Reid et al. (2019) one; this leads to an average value of $R_{\rm CR} \sim 9.6$ kpc (orange). This result implies that the solar neighbourhood is likely within the influence of the Galactic bar, and is in conflict with previous estimates, which suggest a corotation radius of $R_{\rm CR} \sim 5 - 8$ kpc. Moreover, the radius at which the $\Omega_{\rm bar} - \kappa/4$ profile crosses with the pattern speed demarks the ultra-harmonic resonance. We find this to be $R_{\rm UHR} \sim 6.4$ for when assuming either of the two rotation curves used.

参考：先行研究



Bensby et al. (2017) Fig 20
inner Galaxy に若い星(青点)ももまばらに存在していると主張。